

# RetroComposer: Discovering Novel Reactions by Composing Templates for Retrosynthesis Prediction

Chaochao Yan <sup>1</sup>, Peilin Zhao <sup>2</sup>, Chan Lu <sup>2</sup>, Yang Yu <sup>2</sup>, Junzhou Huang <sup>1</sup>

University of Texas at Arlington <sup>1</sup> Tencent AI Lab <sup>2</sup>

## Abstract

The main target of retrosynthesis is to recursively decompose desired molecules into available building blocks. Existing template-based retrosynthesis methods follow a template selection stereotype and suffer from the limited training templates, which prevents them from discovering novel reactions. To overcome the limitation, we propose an innovative retrosynthesis prediction framework that can compose novel templates beyond training templates. So far as we know, this is the first method that can find novel templates for retrosynthesis prediction. Besides, we propose an effective reactant candidates scoring model that can capture atom-level transformation information, and it helps our method outperform existing methods by a large margin. Experimental results show that our method can produce novel templates for 328 test reactions in the USPTO-50K dataset, including 21 test reactions that are not covered by the training templates.

## 1 Introduction

Retrosynthesis plays a significant role in the organic synthesis planning, in which target molecules are recursively decomposed into available commercial building blocks. This analysis mode was firstly formulated in the pioneering work (Corey and Wipke 1969; Corey 1991) and now is one of the fundamental paradigms in the modern chemical society. Since then numerous retrosynthesis prediction algorithms have been proposed to aid or even automate the retrosynthesis analysis. However, the performance of existing methods is still not satisfactory. The massive search space is one of the major challenges of retrosynthesis considering that the order of  $10^7$  compounds and reactions (Gothard et al. 2012) have been reported in the synthetic-organic knowledge. The other challenge is that there are often multiple viable retrosynthesis pathways and it is challenging decide the most appropriate route since the feasibility of a route is often compounded by multiple factors, such as reaction conditions, reaction yield, potential toxic byproducts, and the availability of potential reactants (Yan et al. 2020).

Most of existing machine-learning empowered retrosynthesis methods focus on the single-step version. These methods are broadly grouped into template-based and template-free major categories. Templates-free methods (Liu et al. 2017; Zheng et al. 2020; Yan et al. 2020; Shi et al. 2020;

Tetko et al. 2020; Sacha et al. 2021) rely on deep learning models to directly generate reactants. One effective strategy is to formulate the retrosynthesis prediction as a sequence translation task, and generate SMILES sequences directly using sequence-to-sequence models (Liu et al. 2017; Zheng et al. 2020). SCROP (Zheng et al. 2020) propose to use a second Transformer to correct the initial wrong predictions. Translation-based methods are simple and effective, but lack interpretability behind the prediction. Another representative paradigm is to first find a reaction center within the target which is later split accordingly to obtain hypothetical units named synthons, and then generate reactants incrementally from these synthons (Yan et al. 2020; Shi et al. 2020; Somnath et al. 2021; Wang et al. 2021).

On the other hand, template-based methods are now receiving less attention as the surge of template-free methods. Template-based methods conduct retrosynthesis based on either hand-encoded rules (Szymkuć et al. 2016) or automatically extracted retrosynthesis templates (Coley et al. 2017). Templates encode the minimal reaction transformation patterns, and are straightforwardly interpretable. The key procedure is to select applicable templates to apply to targets (Coley et al. 2017; Segler and Waller 2017b; Segler, Preuss, and Waller 2018; Dai et al. 2019). However, template-based methods have been criticised for the limitation that they can only infer reactions covered by training templates and can not discover novel reactions (Segler and Waller 2017a; Yan et al. 2020). Besides, as the dataset enlarges, the total number of training templates increases at the same time. It is impractical to deploy these retrosynthesis models on large datasets due to the scalability issue.

In this work, we propose a novel template-based single-step retrosynthesis framework to overcome the mentioned limitation. Unlike previous methods only selecting from extracted training templates, we propose to compose templates from basic template building blocks extracted from training templates. In this way, the template selection can be decomposed into a sequential subgraph selection which is more scalable since the selection range at each step is smaller than the total number of templates. Specifically, our method composes templates by first selecting appropriate building blocks iteratively, and then annotate the transformations between the product and reactant atoms. The reaction space of our method is the exponential combination of these extracted

building blocks. This strategy enables our method discover novel templates from training building blocks. What is more, we design an effective reactant scoring model that can capture atom-level transformation information. Thanks to the scoring model, our method outperforms previous methods on the USPTO-50K test dataset. Our contributions are summarized as:

- We propose a first-ever template-based retrosynthesis framework to compose templates, which can discover novel reactions beyond the training data.
- We design an effective reactant scoring model that can capture atom-level transformations, and it contributes significantly to the superiority of our method.
- The proposed method achieves 64.2% and 53.3% Top-1 accuracy on the USPTO-50K test dataset with and without reaction types, respectively, outperforming the previous best published results 63.2% and 52.6%, respectively.

## 2 Related Work

Recently there has been an increasing number of work using machine learning methods to solve the retrosynthesis problem. These methods can be categorized into template-based (Coley et al. 2017; Segler and Waller 2017b; Segler, Preuss, and Waller 2018; Baylon et al. 2019; Dai et al. 2019) and template-free approaches. Template-based methods extract templates from training data and build models to learn the corresponding relationship between products and templates. RetroSim (Coley et al. 2017) selects the templates based on the fingerprint similarity between products and reactions. NeuralSym (Segler and Waller 2017b) uses a neural classification model to select corresponding templates. However, this method does not scale well with increasing number of templates. To mitigate the problem, (Baylon et al. 2019) adopts a multi-scale classification model to select templates according to a manually defined template hierarchy. GLN (Dai et al. 2019) proposes a graph logic network to model the decomposed template hierarchy by first selecting reaction centers within the targets and then only consider templates that contain the selected reaction centers. The decomposition strategy can reduce the search space significantly. GLN can model the reactants and templates jointly by applying selected templates to get reactants which are also used to optimize the model simultaneously.

Template-free methods do not rely on retrosynthesis templates. Instead, they construct models to predict reactants from products directly. Translation based methods (Liu et al. 2017; Zheng et al. 2020; Tetko et al. 2020; Mao et al. 2021) use SMILES to represent molecules and treat the problem as a sequence-to-sequence task. MEGAN (Sacha et al. 2021) treats the retrosynthesis problem as a graph transformation task, and train the model to predict a sequence of graph edits that can transform the product into the reactants. To imitate a chemist’s approach to the retrosynthesis, two-step methods (Shi et al. 2020; Yan et al. 2020; Wang et al. 2021; Somnath et al. 2021) first perform reaction center recognition to obtain synthons by disconnecting targets according to the

reaction center, and then generate reactants from the synthons. G2Gs (Shi et al. 2020) treats the reactant generation process as a series of graph editing operations and utilizes a variational graph generation model to implement the generation process. RetroXpert (Yan et al. 2020) converts the synthon into SMILES to generate reactants as a translation task. GraphRetro (Somnath et al. 2021) also adopts a similar framework and generates the reactants by attaching leaving groups to synthons.

## 3 Preliminary Knowledge

### 3.1 Molecule Graph Representation

The graph representation of a molecule or subgraph pattern is denoted as  $G(\mathcal{V}, \mathcal{E})$ , where  $\mathcal{V}$  and  $\mathcal{E}$  are the set of graph nodes (atoms) and edges (bonds), respectively. Following previous work (Dai et al. 2019; Yan et al. 2020), each bond is represented as two directed edges. Initial node and edge features can be easily collected for the learning purpose.

### 3.2 Graph Attention Networks

Graph Neural Networks (Gilmer et al. 2017) are especially good at learning node- and graph-level embeddings of molecule data. In this work, we adapt the Graph Attention Networks (GATs) (Veličković et al. 2018) to incorporate edge features. The GAT layer updates a node embedding by aggregating its neighbor’s information. The modified GAT concatenates edge embeddings with the associated incoming node embeddings before each graph message passing. The input of the GAT layer is node embeddings  $\{v_i | \forall i \in \mathcal{V}\}$  and edge features  $\{e_{i,j} | (i,j) \in \mathcal{E}\}$ , and the output updated node embeddings  $\{v'_i | \forall i \in \mathcal{V}\}$ . Each node embedding is updated with a shared parametric function  $t_\theta$ :

$$v'_i = t_\theta(v_i, \text{AGGREGATE}(\{[v_j || e_{i,j}] | \forall j \in \mathcal{N}(i)\})), \quad (1)$$

where  $\mathcal{N}(i)$  are neighbor nodes of  $v_i$  and  $||$  is the concatenation operation. The AGGREGATE of GAT adopts an attention-based mechanisms to adaptively weight the neighbor information. A scoring function  $c(i, j)$  computes the importance of the neighbor node  $j$  to node  $i$ :

$$c(i, j) = \text{LeakyReLU}(w^T [\mathbf{W}_1 v_i || \mathbf{W}_1 v_j || \mathbf{W}_2 e_{i,j}]), \quad (2)$$

where  $w$  is a learnable vector parameter and  $\mathbf{W}$  is a learnable matrix parameter. These importance scores are normalized using the Softmax function across the neighbor nodes  $\mathcal{N}(i)$  of the node  $i$  to get attention weights:

$$\alpha(i, j) = \text{Softmax}_j(c(i, j)) = \frac{\exp(c(i, j))}{\sum_{j' \in \mathcal{N}_i} \exp(c(i, j'))}. \quad (3)$$

The modified GAT layer updates the node embedding as the non-linear function  $\sigma$  activated weighted-average of the transformed embeddings of its neighbor nodes:

$$v'_i = \sigma(\sum \alpha(i, j) \mathbf{W}_3 [\mathbf{W}_1 v_j || \mathbf{W}_2 e_{i,j}]). \quad (4)$$

GAT is usually stacked by multiple layers and enhanced with multi-head attention (Vaswani et al. 2017). Please refer to (Veličković et al. 2018) for more details.

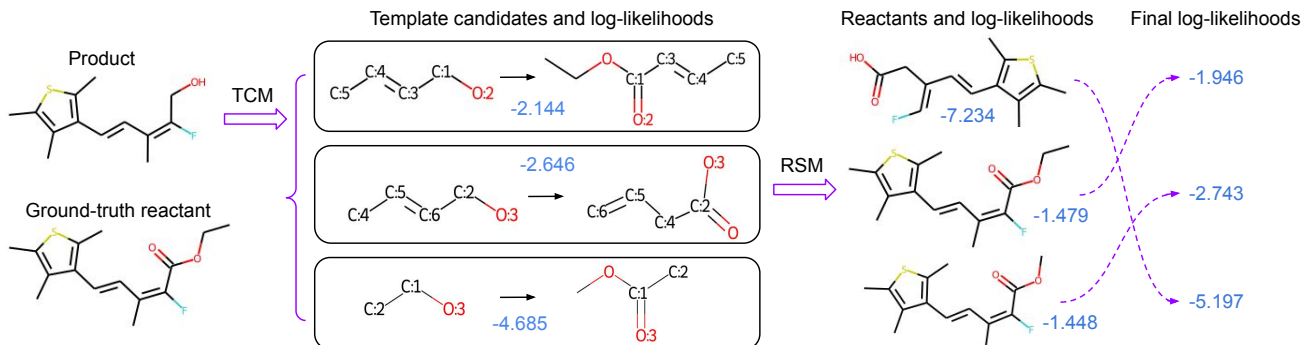


Figure 1: The overall pipeline of our proposed method. Given the desired product as shown at the top left, single-step retrosynthesis is to find the ground-truth reactant as shown at the bottom left. The first stage of our method is to generate a bunch of template candidates (the second column) with our **TCM**. In the second stage, these templates are applied to the product to obtain the reactants (the third column), and then we evaluate each reactant with **RSM**. Numbers indicated in blue are the corresponding log-likelihoods of our models, and the log-likelihoods of **TCM** and **RSM** are combined to get the final ranking of the reactants. In this example, combining the log-likelihoods of **TCM** and **RSM** helps to find the correct Top-1 reactant.

### 3.3 Graph-level Embedding

After obtaining the output node embeddings  $\{v_{i,L}|\forall i \in \mathcal{V}\}$  with a  $L$ -layer GAT, a graph READOUT operation can be used to obtain the graph-level embedding:

$$\text{emb}_G = \text{READOUT}(\{v_{i,L}|\forall i \in \mathcal{V}\}). \quad (5)$$

The READOUT can be any permutation-invariant operation (e.g., mean, sum, max). We adopt the global soft attention layer from (Li et al. 2015) as the READOUT function for molecule graphs due to its excellent performance.

## 4 Method Overview

We propose to compose retrosynthesis templates  $\mathcal{T}$  from a predefined set of template building blocks, and then these composed templates are applied to target products  $\mathcal{P}$  to obtain the associated reactants  $\mathcal{R}$ . Unlike previous template-based methods (Coley et al. 2017; Segler and Waller 2017b; Segler, Preuss, and Waller 2018; Dai et al. 2019) only selecting from training templates, our method can potentially find novel templates which are beyond the training templates. To further improve the retrosynthesis prediction performance, we design a scoring model to evaluate the matches of product and candidate reactants pair. The scoring procedure acts as a verification step, and it plays a significant role in our method. Our scoring model is advantageous since it operates on the atom-level embeddings and is sensitive to local transformations between the product and reactants, while existing methods (Dai et al. 2019) take the molecule-level representations as the input and therefore have a weaker distinguishing ability. The predicted reactants are finally ranked according to the combined log-likelihood of these two stages.

The overall pipeline of our method is shown in Figure 1. The first stage of our method is to compose retrosynthesis templates with a template composer model (**TCM**), which composes retrosynthesis templates by selecting and then assembling template building blocks. In the second stage, the obtained templates are applied to the target product to generate associated reactants. We also summarize the inference

procedure of reactants prediction in the Algorithm 1. After that, we utilize a powerful reactant scoring model (**RSM**) to evaluate generated reactants for each product. During evaluation, the probability scores of both stages are linearly combined to rank reactants prediction. In the following sections, we will detail each stage of our method.

## 5 Compose Retrosynthesis Templates

The template-based retrosynthesis methods are criticized for their limitation to not generalize to reactions of which templates are not within training data, since all existing template-based methods follows the similar procedure to select applicable templates from the extracted training ones.

To overcome the above limitation, we propose a different pipeline to select product and reactant subgraphs sequentially from the corresponding subgraph vocabularies. These selected subgraphs are then assembled into templates with properly assigned atom mappings as illustrated in Figure 2. As far as we know, this is the first attempt to compose retrosynthesis templates instead of selecting the templates. During evaluation, beam search algorithm (Tillmann and Ney 2003) is utilized to find predicted templates.

### 5.1 Subgraph Selection

We denote a subgraph pattern as  $f$ , the product and reactant subgraph set of a template as  $\mathcal{F}_p$  and  $\mathcal{F}_r$ , respectively, and the product and reactant subgraph vocabulary  $\mathcal{F}_P$  and  $\mathcal{F}_R$ , respectively. As shown in Figure 2(c), a retrosynthesis template is composed of product subgraph set  $\mathcal{F}_p$  indicating the reaction center, reactant subgraph set  $\mathcal{F}_r$ , and necessary mapping numbers specifying the atom transformation relationship between the product and reactant molecules.

To build product subgraph vocabulary  $\mathcal{F}_P$  and reactant subgraph vocabulary  $\mathcal{F}_R$ , retrosynthesis templates extracted from training data are split into separate subgraphs to collect unique subgraph patterns. We build separate vocabularies for the product and reactant subgraphs due to their essential difference. Product subgraphs represent reaction centers

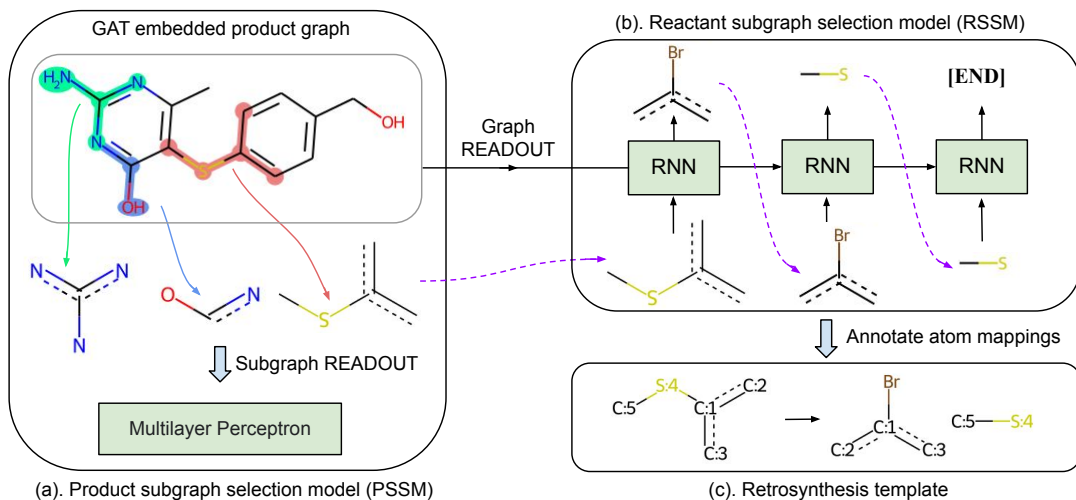


Figure 2: The workflow of our template composer model (TCM): (a) selecting a proper product subgraph with **PSSM**, (b) selecting reactant subgraphs sequentially with **RSSM**, and (c) annotating atom mappings between the product subgraph and the reactant subgraphs to obtain a template. In **PSSM**, the product is firstly embedded by a GAT, then the embeddings of contained subgraphs are obtained via the subgraph READOUT operation. These embeddings are fed into a multilayer perceptron (MLP) for product subgraph selection. The hidden state of RNN in **RSSM** is initialized from the product graph READOUT, and the start token is the selected product subgraph. At each time step, a reactant subgraph is generated until the [END].

and are more generalizable, while reactant subgraphs may contain extra leaving groups which are more specific to the reaction class and the desired product. We find this strategy works pretty well in practice.

**Product Subgraph Selection** To compose retrosynthesis templates for a desired target, the first step is to choose proper  $\mathcal{F}_p$  from the vocabulary  $\mathcal{F}_P$ . In this work, we focus on the single-product reactions, therefore  $\mathcal{F}_p$  actually consists of a single subgraph pattern  $f$ . Note that there may be multiple viable retrosynthesis templates for each reaction, so each target may have several applicable product subgraphs  $\mathcal{F}_a$ . Since each product graph  $G_p$  contains only a limited set of predefined candidate subgraphs  $\mathcal{F}_c$ , we only need to consider the candidate subgraphs  $\mathcal{F}_c$  to guide the selection process (Dai et al. 2019). Here  $\mathcal{F}_a \subseteq \mathcal{F}_c \subseteq \mathcal{F}_P$ .

In this situation, the product subgraph selection can be regarded as a multi-label classification problem. However, it is not optimal to train the product subgraph selection model (**PSSM**) with binary cross-entropy loss as in the multi-label classification setting, since (1) it predicts the applicability score independently for each  $f \in \mathcal{F}_c$  without considering the interrelationship and (2) the constraint is too strong to try to classify every  $f \in \mathcal{F}_c$  correctly. Note that the absolute applicability scores of subgraphs in  $\mathcal{F}_c$  do not matter here, what really matters is the ranking of these applicability scores since the beam search is adopted to find a series of template candidates during evaluation. Softmax classifier can consider the relationship of all subgraphs in  $\mathcal{F}_c$ , but it can not be directly applied to **PSSM**, since it is not suitable for the multi-label case. Inspired by Softmax, we propose to optimize **PSSM** with following negative log-likelihood loss:

$$L_{\text{PSSM}} = -\log\left(\frac{\text{mean}(o^{\mathcal{F}_a})}{\text{mean}(o^{\mathcal{F}_a}) + \text{sum}(o^{\mathcal{F}_c \setminus \mathcal{F}_a})}\right), \quad (6)$$

where  $o^{\mathcal{F}}$  is the exponential of **PSSM** output logits for subgraphs in  $\mathcal{F}$  and  $\setminus$  is set subtraction. In the above loss function, the exponential output for all subgraphs in  $\mathcal{F}_a$  is averaged in the numerator, which is considered as the exponential of ground-truth class output before normalization in the Softmax classifier. The extra item in denominator is the summation of exponential output of all inapplicable subgraphs in  $\mathcal{F}_c$ . The intuition is that any applicable product subgraph is found during evaluation should be fine, so the **PSSM** is driven to output larger over all  $o^{\mathcal{F}_a}$  than all outputs in  $o^{\mathcal{F}_c \setminus \mathcal{F}_a}$ . The constraint is more relaxed and it works better than binary cross-entropy loss in our experiments.

In our method, **PSSM** scores each contained subgraph  $f \in \mathcal{F}_c$  based on the subgraph embeddings. As shown in Figure 2(a), to obtain the subgraph embeddings, the nodes of product molecule graph  $G_p$  are first encoded with the GAT. The embedding  $\text{emb}_f$  of the contained subgraph  $f$  is gathered as the average embedding of  $G_f$  associated nodes within  $G_p$ , and then these embeddings are fed into a MLP. Here for the subgraph  $f$ , the READOUT is implemented as the arithmetic average for its simplicity and efficiency, and it can also be other order invariant aggregations. Note that this is different from GLN (Dai et al. 2019) in which  $G_p$  and  $G_f$  are considered as two graphs and embedded separately. Our strategy to reuse node embeddings is more efficient and can learn more informative  $\text{emb}_f$  since the neighboring structure of  $G_f$  within  $G_p$  are also incorporated during the message passing. Besides, our method can naturally handle multiple equivalent subgraphs situation in which  $G_f$



appears multiple times within  $G_p$ .

**Reactant Subgraph Selection** The second step of the subgraph selection is to choose a set of reactant subgraphs  $\mathcal{F}_r$  from the vocabulary  $\mathcal{F}_R$ , which is ordered according to the subgraph frequency in training data so that  $\mathcal{F}_r$  is also ordered. With minor notation abuse,  $\mathcal{F}_r$  also denotes an ordered sequence of reactant subgraphs in the following content.

We build the reactant subgraph selection model (**RSSM**) based on the recurrent neural network (RNN) as illustrated in Figure 2(b), and formulate subgraph selection as a classification task at each RNN time step. The hidden state of RNN is initialized from the product graph READOUT and the start token is  $f_p$ , as well as an extra end token [END] is appended to reactant subgraph sequence  $\mathcal{F}_r$ .

For the start token  $f_p$ , we reuse product subgraph embeddings obtained previously since it provides better performance than embedding the token in the traditional manner.

## 5.2 Annotate Atom Mappings

Given  $f_p$  and  $\mathcal{F}_r$ , the final step is to annotate the atom mappings between  $f_p$  and  $\mathcal{F}_r$  to obtain the retrosynthesis template. A subgraph pattern  $f$  is represented in the SMARTS string, and we use open source toolkit Indigo<sup>1</sup>’s `automap()` function to build atom mappings. We empirically find about 70% of USPTO-50K training templates can be successfully annotated with correct atom mappings. To remedy this deficiency, we keep a memo of training templates and associated  $f_p$  and  $\mathcal{F}_r$ . Note that each subgraph combination may be associated to multiple templates due to the uncertainty of atom transformations. During evaluation, the predicted  $f_p$  and  $\mathcal{F}_r$  are processed with `automap()` only when not found in the memo. In future, we may try to annotate atom mappings using other tools such as RXNMapper (Schwaller et al. 2021).

## 6 Score Reactant Prediction

After a retrosynthesis template is composed, reactants can be easily obtained by applying the template to the target using RDKit<sup>2</sup>’s `RunReactants()` or RDChiral<sup>3</sup>’s `run_reaction()` function. To achieve superior retrosynthesis prediction performance, it is important to verify that the predicted reactants can generate the target successfully before the final evaluation. The reactant prediction scoring is formulated as a multi-class classification task.

To serve the verification purpose, we build a reactant scoring model (**RSM**) based on GATs.  $G_p$  and  $G_r$  are first input into a GAT to learn node embeddings. Note that target and the generated reactants are atom-mapped, therefore for each node in  $G_p$  we can easily find its corresponding node in  $G_r$ . Inspired by WLDN (Jin et al. 2017), we define a fusion function  $F(n_a^p, n_{a'}^r)$  to combine the node embeddings of product node  $a$  and its associated reactant node  $a'$ .

The fused node embeddings are regarded as the new node features of  $G_p$ , which is input into another GAT to learn the

---

### Algorithm 1: Reactants prediction algorithm

---

**Input:** Target molecule graph, candidate product subgraphs  
**Output:** A sequence of reactants

```

1: Input the target molecule graph into the GAT.
2: Perform graph READOUT to get the target embedding as the Equation (5).
3: Perform subgraph READOUT to get the embeddings.
4: for each product subgraph  $f_p$  do
5:   Initialize RNN hidden state from target embedding.
6:   Input the embedding of subgraph  $f_p$  into the RNN.
7:   if RNN output is [END] then
8:     Terminate the RNN decoding for  $f_p$ .
9:     Annotate mapping numbers between product subgraph and reactant subgraphs to get a template.
10:    if template is valid then
11:      Apply the template to get reactants, and store the reactants in the result.
12:    end if
13:  else
14:    Embed output  $f_r$  as RNN input at next time-step.
15:  end if
16: end for
17: return The collected sequence of reactants.
```

---

graph-level embedding  $emb_G = \text{READOUT}(\{n_a | \forall a \in G_p\})$ . In this way, the critical difference between the product and reactants can be better captured since our **RSM** can incorporate higher order interactions between these fused node embeddings through the graph message passing process.

The graph-level embedding is then fed into a simple MLP composed of two fully-connected layers to output a compatibility score. The final probability score is obtained by applying a Softmax function to the compatibility scores of all candidate reactants associated to the target.

The log-likelihood of **TCM** and **RSM** predictions are denoted as  $l_{TCM}$  and  $l_{RSM}$ , respectively. The predicted reactants are finally ranked according to the linear combination value of  $\lambda * l_{TCM} + (1 - \lambda) * l_{RSM}$ ,  $0 \leq \lambda \leq 1$ . The optimal hyper-parameter  $\lambda$  can be determined by the validation.

### 6.1 Fusion Functions

Three different fusion functions  $F_1, F_2$ , and  $F_3$  are implemented and investigated in our experiments:

$$F(n_a^p, n_{a'}^r) = \begin{cases} n_a^p - n_{a'}^r & F_1 \\ \mathbf{W}_4(n_a^p - n_{a'}^r) || \mathbf{W}_5(n_a^p + n_{a'}^r) & F_2 \\ \mathbf{W}_4(n_a^p - n_{a'}^r) || \mathbf{W}_5(\bar{n}_a^p * \bar{n}_{a'}^r) & F_3 \end{cases} \quad (7)$$

where  $||$  indicates the concatenation operation,  $\bar{n}$  denotes the L2-normalized node embedding, and  $\mathbf{W}$  is a matrix that halves node embedding dimension so that the concatenated embedding restores the original dimension.

The benefit of taking the difference of node embeddings is that the fusion embeddings deviates from zero only if it is close to the reaction center (Jin et al. 2017), therefore the **RSM** can focus on the transformed atoms and their immediate neighbors. However,  $F_1$  only considers the difference

<sup>1</sup><https://github.com/epam/Indigo>

<sup>2</sup><https://github.com/RDKit/RDKit>

<sup>3</sup><https://github.com/connorcoley/rdchiral>

while ignoring the absolute value. We propose to also concatenate the summation term as the  $F_2$ , and the multiplication term as the  $F_3$ . In our method, we adopt the fusion function  $F_2$  due to its best performance as shown in our experiments.

## 7 Experiment

### 7.1 Dataset and Preprocessing

Our method is evaluated on the standard benchmark dataset USPTO-50K (Schneider, Stiefl, and Landrum 2016) under two settings to demonstrate its effectiveness. USPTO-50K is derived from USPTO granted patents (Lowe 2012), and it is composed of 50K reactions annotated with 10 reaction types. We split reaction data into training/validation/test sets in 8:1:1 the same way as previous work (Coley et al. 2017; Dai et al. 2019). Since the original annotated mapping numbers in the USPTO dataset may result in unexpected information leakage<sup>4</sup>, we first preprocess the USPTO reactions to re-assign product mapping numbers according to its canonical atom order as suggested by (Yan et al. 2020). The atom and bond features are similar to the previous work (Yan et al. 2020), and reaction types are converted into one-hot vectors concatenated with the original atom features. Details about atom and bond features can be found in the supplementary.

Following (Yan et al. 2020), we extract templates from training reactions using RDChiral (Coley, Green, and Jensen 2019). We obtain 10212 unique templates in total for the USPTO-50K training data, and 93.7% of test reactions are covered by these templates. The gathered templates are split into product and reactant subgraphs of which mapping numbers are further removed to obtain the subgraph vocabularies.

For each target, we find all occurred subgraphs set  $\mathcal{F}_c$  using graph matching algorithms as well as all applicable templates by trying to apply possible templates to see if the ground-truth reactants can be obtained. The applicable subgraphs  $\mathcal{F}_a$  can be obtained easily from the acquired applicable templates. Since the graph matching process might be time-consuming, we extract the fingerprint for each molecule/sub-molecule to filter those impossible subgraphs. For the subgraph screening purpose, we adopt the PatternFingerprint from RDKit and use a fingerprint size of 1024. Following previous methods we use beam search to find top-50 template predictions during evaluation, which are applied to targets to collect candidate reactants. The gathered targets and candidate reactants are the experimental data for the **RSM**.

### 7.2 Implementation

Our model is implemented using PyTorch (Paszke et al. 2019) and PyTorch Geometric (Fey and Lenssen 2019) library. The adapted GAT model is built based on the source implementation of Pretrain-GNN (Hu et al. 2019). We use the same GAT model settings in all tasks, except that the number of GAT layers is 6 in **TCM** while 3 in **RSM**. The embedding dimension is set as 300 for all embeddings for

Table 1: Test retrosynthesis results comparison with the existing methods. The best results are shown in bold. \*RetroXpert results are updated by the authors due to information leakage.

Methods	Top- <i>n</i> accuracy (%)					
	1	3	5	10	20	50
USPTO-50K without reaction types						
RetroSim	37.3	54.7	63.3	74.1	82.0	85.3
NeuralSym	44.4	65.3	72.4	78.9	82.2	83.1
SCROP	43.7	60.0	65.2	68.7	-	-
GLN	52.6	68.0	75.1	83.1	88.5	92.1
G2Gs	48.9	67.6	72.5	75.5	-	-
RetroXpert*	50.4	61.1	62.3	63.4	63.9	64.0
MEGAN	48.1	70.7	78.4	86.1	<b>90.3</b>	<b>93.2</b>
Ours	<b>53.3</b>	<b>75.2</b>	<b>80.9</b>	85.0	86.1	86.2
USPTO-50K with given reaction types						
RetroSim	52.9	73.8	81.2	88.1	91.8	92.9
NeuralSym	55.3	76.0	81.4	85.1	86.5	86.9
SCROP	59.0	74.8	78.1	81.1	-	-
GLN	63.2	77.5	83.4	89.1	92.1	93.2
G2Gs	61.0	81.3	86.0	88.7	-	-
RetroXpert*	62.1	75.8	78.5	80.9	82.8	83.5
MEGAN	60.7	82.0	87.5	<b>91.6</b>	<b>93.9</b>	<b>95.3</b>
Ours	<b>64.2</b>	<b>84.2</b>	<b>88.1</b>	89.7	90.0	90.1

simplicity. The **TCM** is trained with batch size 32 and Adam (Kingma and Ba 2014) optimizer with default settings, and the initial learning rate is  $3e^{-4}$ . The learning rate is adjusted with CosineAnnealingLR. We adopt the GRU (Cho et al. 2014) as the RNN implementation in **TCM**, the number of GRU layers is 2 and both its embedding and hidden size are 300. The model is trained in multi-process mode on a single GTX 1080 Ti GPU for acceleration. It takes about two hours to train the **TCM** for 80 epochs. The **RSM** training costs about 6 hours for 20 epochs. The final model parameters are saved and later loaded for inference. We run all experiments for three times and report the mean performance in default. More detailed settings are included in the supplementary.

### 7.3 Evaluation Metric

Top-K accuracy is adopted as the evaluation metric for the retrosynthesis prediction. The generated reactants are converted into canonical SMILES, and if and only counts as a successful hit when they are the same as the ground-truth.

## 8 Main Results

### 8.1 Retrosynthesis Prediction Performance

We compare our proposed method RetroComposer with existing methods on the USPTO-50K dataset, and report results in Table 1. For both evaluation settings (w/ and w/o reaction types), our method outperforms previous methods

<sup>4</sup><https://github.com/uta-smile/RetroXpert>

by a significant margin and achieves the best accuracy in the Top-1, Top-3, and Top-5. Specially, without reaction types, our RetroComposer achieves 53.3% Top-1 accuracy which outperforms the current best published GLN (Dai et al. 2019) by 0.7%. When the reaction types are specified, our method also obtains the test Top-1 accuracy 64.2%, and it outperforms the existing best method GLN by 1.0%. The superior performance demonstrates the effectiveness of our method. Particularly, the superiority of our method is more significant in real world applications where reaction types are unknown.

What is more, our Top-10 accuracy is already quite high, and the extra Top-50 predictions bring only minor improvements (85.0%  $\rightarrow$  86.2% and 89.7%  $\rightarrow$  90.1%). It indicates that our method can usually find the best reactant sets for the targets in a few candidates. This is especially important for the multi-step retrosynthesis, in which the number of generated reaction paths will grow exponentially with the path length. We also notice that GLN achieves better Top-50 accuracy than our method, this is because our method is less constrained and has a much larger template space to search.

## 8.2 Novel Templates

Different from existing methods, our method can find novel templates that are not in training data. Our model predicts different templates based on different possible reaction center of a given target. For example, an amide formation template and alkylation template may both be applied in one target, and our model can predict suitable templates very well and give reasonable corresponding reactants for such cases. For the type conditional setting, our model obtains novel templates for 328 unique targets that generate the ground-truth reactants. For 6.3% of test reactions that are not covered by train templates, our algorithm can predict relevant templates very well for most of reaction types, although it fails in some heterocyclic formation reactions. This is because there are very few of such reaction data in USPTO-50K. Particularly, our method successfully discovers viable templates for 21 uncovered test reactions, which confirms that our method can find novel reactions. Two of such examples are illustrated in Figure 3.

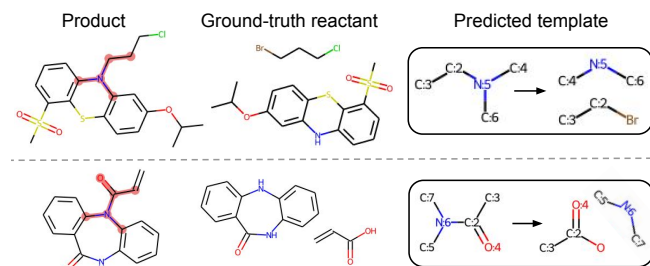


Figure 3: Our method successfully finds valid templates for two test reactions that are not covered by training data. The matched product subgraph is highlighted in pink within the product graph for better visualization.

Table 2: Top-1 accuracy (%) with different  $\lambda$  values.

$\lambda$	0	0.2	0.3	0.4	0.9	1.0
Wo/ types	51.0	52.9	<b>53.3</b>	53.0	50.3	48.1
W/ types	62.9	63.9	<b>64.2</b>	63.8	61.7	58.9

## 8.3 Ablation Study

We set  $\lambda = 0.3$  for both settings according to the validation performance. Ablation study results of hyper-parameter  $\lambda$  are shown in Table 2. Note that with only TCM ( $\lambda = 1.0$ ), the performance has an appreciable gap with the existing methods. The  $l_{RSM}$  indicates the likelihood of retrosynthesis templates, while  $l_{TCM}$  scores each reaction by looking at the detailed atom transformations. These two terms are complementary and combined to achieve the best performance.

## 9 Conclusion

In this work, we propose a novel template-based retrosynthesis prediction framework that composes templates by selecting and assembling molecule subgraphs. Experimental results confirm that the proposed strategy can discover novel reactions, and achieve comparable retrosynthesis accuracy. To further improve the ranking accuracy, we present a novel reactant scoring model to rank candidate reactants by taking into account the atom-level transformations. Our method significantly outperforms previous methods and sets new SOTA performance on the USPTO-50K test dataset, which proves the effectiveness of our method.

## References

- Baylon, J. L.; Cilfone, N. A.; Gulcher, J. R.; and Chittenden, T. W. 2019. Enhancing retrosynthetic reaction prediction with deep learning using multiscale reaction classification. *Journal of chemical information and modeling*, 59(2): 673–688.
- Cho, K.; Van Merriënboer, B.; Bahdanau, D.; and Bengio, Y. 2014. On the properties of neural machine translation: Encoder-decoder approaches. *arXiv preprint arXiv:1409.1259*.
- Coley, C. W.; Green, W. H.; and Jensen, K. F. 2019. RD-Chiral: An RDKit wrapper for handling stereochemistry in retrosynthetic template extraction and application. *Journal of chemical information and modeling*, 59(6): 2529–2537.
- Coley, C. W.; Rogers, L.; Green, W. H.; and Jensen, K. F. 2017. Computer-assisted retrosynthesis based on molecular similarity. *ACS central science*, 3(12): 1237–1245.
- Corey, E. J. 1991. The logic of chemical synthesis: multistep synthesis of complex carbogenic molecules (Nobel Lecture). *Angewandte Chemie International Edition in English*, 30(5): 455–465.
- Corey, E. J.; and Wipke, W. T. 1969. Computer-assisted design of complex organic syntheses. *Science*, 166(3902): 178–192.

- Dai, H.; Li, C.; Coley, C.; Dai, B.; and Song, L. 2019. Retrosynthesis Prediction with Conditional Graph Logic Network. In *Advances in Neural Information Processing Systems*, 8870–8880.
- Fey, M.; and Lenssen, J. E. 2019. Fast graph representation learning with PyTorch Geometric. *arXiv preprint arXiv:1903.02428*.
- Gilmer, J.; Schoenholz, S. S.; Riley, P. F.; Vinyals, O.; and Dahl, G. E. 2017. Neural message passing for quantum chemistry. In *Proceedings of the 34th International Conference on Machine Learning-Volume 70*, 1263–1272. JMLR.org.
- Gothard, C. M.; Soh, S.; Gothard, N. A.; Kowalczyk, B.; Wei, Y.; Baytekin, B.; and Grzybowski, B. A. 2012. Rewiring chemistry: Algorithmic discovery and experimental validation of one-pot reactions in the network of organic chemistry. *Angewandte Chemie International Edition*, 51(32): 7922–7927.
- Hu, W.; Liu, B.; Gomes, J.; Zitnik, M.; Liang, P.; Pande, V.; and Leskovec, J. 2019. Strategies for pre-training graph neural networks. *arXiv preprint arXiv:1905.12265*.
- Jin, W.; Coley, C.; Barzilay, R.; and Jaakkola, T. 2017. Predicting organic reaction outcomes with weisfeiler-lehman network. In *Advances in Neural Information Processing Systems*.
- Kingma, D. P.; and Ba, J. 2014. Adam: A method for stochastic optimization. *arXiv preprint arXiv:1412.6980*.
- Li, Y.; Tarlow, D.; Brockschmidt, M.; and Zemel, R. 2015. Gated graph sequence neural networks. *arXiv preprint arXiv:1511.05493*.
- Liu, B.; Ramsundar, B.; Kawthekar, P.; Shi, J.; Gomes, J.; Luu Nguyen, Q.; Ho, S.; Sloane, J.; Wender, P.; and Pande, V. 2017. Retrosynthetic reaction prediction using neural sequence-to-sequence models. *ACS central science*, 3(10): 1103–1113.
- Lowe, D. M. 2012. *Extraction of chemical structures and reactions from the literature*. Ph.D. thesis, University of Cambridge.
- Mao, K.; Xiao, X.; Xu, T.; Rong, Y.; Huang, J.; and Zhao, P. 2021. Molecular graph enhanced transformer for retrosynthesis prediction. *Neurocomputing*, 457: 193–202.
- Paszke, A.; Gross, S.; Massa, F.; Lerer, A.; Bradbury, J.; Chanan, G.; Killeen, T.; Lin, Z.; Gimelshein, N.; Antiga, L.; et al. 2019. Pytorch: An imperative style, high-performance deep learning library. *Advances in neural information processing systems*, 32: 8026–8037.
- Sacha, M.; Błaż, M.; Byrski, P.; Włodarczyk-Pruszyński, P.; and Jastrzebski, S. 2021. Molecule Edit Graph Attention Network: Modeling Chemical Reactions as Sequences of Graph Edits. *Journal of Chemical Information and Modeling*, 61(7): 3273–3284.
- Schneider, N.; Stiefl, N.; and Landrum, G. A. 2016. What’s what: The (nearly) definitive guide to reaction role assignment. *Journal of chemical information and modeling*, 56(12): 2336–2346.
- Schwaller, P.; Hoover, B.; Reymond, J.-L.; Strobelt, H.; and Laino, T. 2021. Extraction of organic chemistry grammar from unsupervised learning of chemical reactions. *Science Advances*, 7(15): eabe4166.
- Segler, M. H.; Preuss, M.; and Waller, M. P. 2018. Planning chemical syntheses with deep neural networks and symbolic AI. *Nature*, 555(7698): 604–610.
- Segler, M. H.; and Waller, M. P. 2017a. Modelling chemical reasoning to predict and invent reactions. *Chemistry–A European Journal*, 23(25): 6118–6128.
- Segler, M. H.; and Waller, M. P. 2017b. Neural-symbolic machine learning for retrosynthesis and reaction prediction. *Chemistry–A European Journal*, 23(25): 5966–5971.
- Shi, C.; Xu, M.; Guo, H.; Zhang, M.; and Tang, J. 2020. A Graph to Graphs Framework for Retrosynthesis Prediction. *arXiv preprint arXiv:2003.12725*.
- Somnath, V.; Bunne, C.; Coley, C.; Krause, A.; and Barzilay, R. 2021. Learning Graph Models for Retrosynthesis Prediction. *arXiv preprint arXiv:2006.07038*.
- Szymkuć, S.; Gajewska, E. P.; Klucznik, T.; Molga, K.; Dittwald, P.; Startek, M.; Bajczyk, M.; and Grzybowski, B. A. 2016. Computer-Assisted Synthetic Planning: The End of the Beginning. *Angewandte Chemie International Edition*, 55(20): 5904–5937.
- Tetko, I. V.; Karpov, P.; Van Deursen, R.; and Godin, G. 2020. State-of-the-art augmented NLP transformer models for direct and single-step retrosynthesis. *Nature communications*, 11(1): 1–11.
- Tillmann, C.; and Ney, H. 2003. Word reordering and a dynamic programming beam search algorithm for statistical machine translation. *Computational linguistics*, 29(1): 97–133.
- Vaswani, A.; Shazeer, N.; Parmar, N.; Uszkoreit, J.; Jones, L.; Gomez, A. N.; Kaiser, Ł.; and Polosukhin, I. 2017. Attention is all you need. In *Advances in neural information processing systems*, 5998–6008.
- Veličković, P.; Cucurull, G.; Casanova, A.; Romero, A.; Liò, P.; and Bengio, Y. 2018. Graph Attention Networks. *International Conference on Learning Representations*.
- Wang, X.; Li, Y.; Qiu, J.; Chen, G.; Liu, H.; Liao, B.; Hsieh, C.; and Yao, X. 2021. RetroPrime: A Diverse, plausible and Transformer-based method for Single-Step retrosynthesis predictions. *Chemical Engineering Journal*, 420: 129845.
- Yan, C.; Ding, Q.; Zhao, P.; Zheng, S.; Yang, J.; Yu, Y.; and Huang, J. 2020. RetroXpert: Decompose Retrosynthesis Prediction Like A Chemist. In *Advances in Neural Information Processing Systems*, volume 33, 11248–11258.
- Zheng, S.; Rao, J.; Zhang, Z.; Xu, J.; and Yang, Y. 2020. Predicting Retrosynthetic Reactions using Self-Corrected Transformer Neural Networks. *Journal of Chemical Information and Modeling*.



# Appendices

## A USPTO-50K dataset information

The USPTO-50K consists of 50K reactions that are annotated with 10 reaction types, and the detailed distribution of reaction types is displayed in the below Table 3. The imbalanced reaction type distribution makes the retrosynthesis prediction more challenging.

Table 3: Distribution of 10 recognized reaction types.

Type	Reaction type name	# Reactions
1	Heteroatom alkylation and arylation	15204
2	Acylation and related processes	11972
3	C-C bond formation	5667
4	Heterocycle formation	909
5	Protections	672
6	Deprotections	8405
7	Reductions	4642
8	Oxidations	822
9	Functional group interconversion	1858
10	Functional group addition (FGA)	231

We can extract 10212 unique templates from the training data, and 93.7% of test reactions are covered by these templates. For each product molecule, there are an average of 42.82 contained subgraphs which are denoted as  $\mathcal{F}_c$  in the section 5.1. Among these subgraphs, there are an average of 2.29 applicable subgraphs denoted as  $\mathcal{F}_a$ . Note that the average number of templates is 2.01, which indicates that for some applicable product subgraphs there are multiple matches in the same product graph. Our method can naturally handle the situation as explained in the section 5.1. More statistical results are included in Table 4.

Table 4: Statistical results of templates and reactions.

# total templates	10212
# unique product subgraphs	7666
# unique reactant subgraphs	4343
Test reactions coverage by training templates	93.7%
Average # contained product subgraphs per mol	43.82
Average # applicable product subgraphs per mol	2.29
Average # templates per reaction	2.01
Average # reactants per reaction	1.71

## B Atom and bond features

Following (Yan et al. 2020), we use similar bond and atom features to build molecule graphs as listed in Table 5 and 6. These features can be easily extracted using RDKit.

Table 5: Bond features used in our method. These features are one-hot encoding.

Feature	Description	Size
Bond type	Single, double, triple, or aromatic.	4
Conjugation	Whether the bond is conjugated.	1
In ring	Whether the bond is part of a ring.	1
Stereo	None, any, E/Z or cis/trans.	6

Table 6: Atom features used in our method. All features are one-hot encoding, except the atomic mass is a real number scaled to be on the same order of magnitude. The reaction type is applicable for type conditional setting.

Feature	Description	Size
Atom type	Type of atom (ex. C, N, O), by atomic number.	17
# Bonds	Number of bonds the atom is involved in.	6
Formal charge	Integer electronic charge assigned to atom.	5
Chirality	Unspecified, tetrahedral CW/CCW, or other.	4
# Hs	Number of bonded Hydrogen atom.	5
Hybridization	sp, sp2, sp3, sp3d, or sp3d2.	5
Aromaticity	Whether this atom is part of an aromatic system.	1
Atomic mass	Mass of the atom, divided by 100.	1
Reaction type	The specified reaction type if it exists.	10

## C Experimental Settings

The **TCM** model is composed of a modified GAT and a simple RNN model. We add a self-loop to each graph node following (Dai et al. 2019; Yan et al. 2020). Both atom and bond features are first converted into embeddings of size 300 through a linear layer. The GAT consists of 6 layers and 2 attention heads for the multi-head attention. Node embeddings output from each layers are concatenated before the graph READOUT operation to increase the representative power. A simple MLP is applied to product subgraph embeddings to select the proper product subgraph. The MLP is composed of two linear layers and a ReLU activation is placed between the two linear layers. We also use a Dropout layer with a dropout rate of 0.3 in the MLP. The **TCM** model is trained on a single GTX-1080 Ti GPU in 4 concurrent processes. The multi-process training significantly speeds up the model training. We take the final model after training for inference since the **TCM** model training converges well.

The **RSM** model is composed of two GATs and a MLP head. Product and reactant graphs are embedded with separate GAT models and the GAT uses the same settings as in the **TCM** except that each GAT is composed of 3 layers now. Note that for reactions with multiple reactants, we regard the disconnected molecule graphs as a single large graph. The composition of the MLP head is similar to that in **RSM**. The **RSM** model is also trained in multi-process mode for acceleration.

We find our model is quite robust to the hyper-parameters, and most of the settings are copied from (Hu et al. 2019) as they are given. We slightly tune the model hyper-parameters such as learning rate and batch size under the type unknown setting, and find the same settings also work well for the type conditional case. The performance for the type conditional case may be further improved if the settings are more customized.